Accepted Manuscript

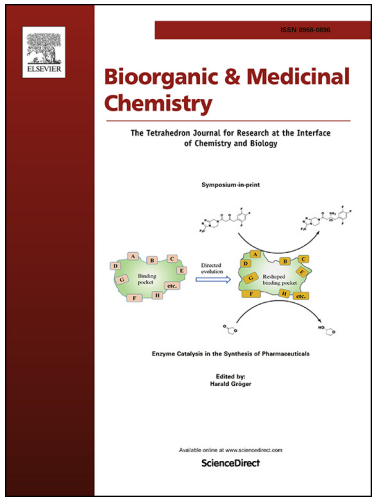

Screening, Synthesis, Crystal Structure, and Molecular Basis of 6-Amino-4-phenyl-1,4-dihydropyrano[2,3-c]pyrazole-5-carbonitriles as Novel AKR1C3 Inhibitors

Xuehua Zheng, Zan Jiang, Xiaolin Li, Chen Zhang, Zhe Li, Yinuo Wu, Xinhua Wang, Chao Zhang, Hai-bin Luo, Jun Xu, Deyan Wu

PII: S0968-0896(18)31389-0
DOI: https://doi.org/10.1016/j.bmc.2018.10.044
Reference: BMC 14603

To appear in: *Bioorganic & Medicinal Chemistry*

Received Date: 3 August 2018
Revised Date: 15 October 2018
Accepted Date: 30 October 2018

Please cite this article as: Zheng, X., Jiang, Z., Li, X., Zhang, C., Li, Z., Wu, Y., Wang, X., Zhang, C., Luo, H-b., Xu, J., Wu, D., Screening, Synthesis, Crystal Structure, and Molecular Basis of 6-Amino-4-phenyl-1,4-dihydropyrano[2,3-c]pyrazole-5-carbonitriles as Novel AKR1C3 Inhibitors, *Bioorganic & Medicinal Chemistry* (2018), doi: https://doi.org/10.1016/j.bmc.2018.10.044

Screening, Synthesis, Crystal Structure, and Molecular Basis of 6-Amino-4-phenyl-1,4-dihydropyrano[2,3-c]pyrazole-5-carbonitriles as Novel AKR1C3 Inhibitors

Xuehua Zheng[a], Zan Jiang[a], Xiaolin Li[b], Chen Zhang[b], Zhe Li[b], Yinuo Wu[b], Xinhua Wang[a], Chao Zhang[a], Hai-bin Luo[b], Jun Xu [b,*], Deyan Wu [b,†]

[a]*Key Laboratory of Molecular Target & Clinical Pharmacology, School of Pharmaceutical Sciences & the Fifth Affiliated Hospital, Guangzhou Medical University, Guangzhou 511436, China*

[b]*School of Pharmaceutical Sciences, Sun Yat-sen University, Guangzhou, 510006, China*

Abstract: AKR1C3 is a promising therapeutic target for castration-resistant prostate cancer. Herein, an evaluation of in-house library discovered substituted pyranopyrazole as a novel scaffold for AKR1C3 inhibitors. Preliminary SAR exploration identified its derivative **19d** as the most promising compound with an IC_{50} of 0.160 μM among the 23 synthesized molecules. Crystal structure studies revealed that the binding mode of the pyranopyrazole scaffold is different from the current inhibitors. Hydroxyl, methoxy and nitro group at the C4-phenyl substituent together anchor the inhibitor to the oxyanion site, while the core of the scaffold dramatically enlarges but partially occupies the SP pockets with abundant hydrogen bond interactions. Strikingly, the inhibitor undergoes a conformational change to fit AKR1C3 and its homologous protein AKR1C1. Our results suggested that conformational changes of the receptor and the inhibitor should both be considered during the rational design of selective AKR1C3 inhibitors. Detailed binding features obtained from molecular dynamics simulations helped to finally elucidate the molecular basis of 6-Amino-4-phenyl-1,4-dihydropyrano[2,3-c]pyrazole-5-carbonitriles as AKR1C3 inhibitors, which would facilitate the future rational inhibitor design and structural optimization.

Key words: AKR1C3 inhibitors; Synthesis; Crystal structure; Castration-resistant prostate cancer; 1,4-dihydropyrano[2,3-c]pyrazole

[*]Corresponding author. Jun Xu, Tel.: +086-020-3994-3023, Fax: +86-20-3994-3000, and E-mail: junxu@biochemomes.com.
Deyan Wu, Tel.: +086-020-3994-3062, Fax: +86-20-3994-3000, and E-mail: wudeyan3@mail.sysu.edu.cn.

1. Introduction

AKR1C3, one member of aldo-keto reductase (AKR) superfamily, has also been designated as 17β-hydroxysteroid dehydrogenase type 5 (17β-HSD5) due to its 17- ketosteroid reductase activity. The substrates of AKR1C3 include the precursors in all pathways to the potent androgens testosterone (T) and 5α-dihydrotestosterone (DHT) in the prostate, such as dehydroepiandrosterone, Δ4-androstene-3,17-dione, androstan-3,17-dione and androsterone[1]. Recent studies have established that the reactivation of the androgen axis contributes to castrate resistant prostate cancer (CRPC), and led to FDA approval of abiraterone (steroidogenic enzyme CYP17A1 inhibitor) and enzalutamide (new androgen receptor antagonist) for the treatment of patients with CRPC[2-4]. The involvement of AKR1C3 in downstream androgen biosynthesis suggests that AKR1C3 plays a critical role in CRPC. Recent investigations have indicated that AKR1C3 is overexpressed in cell lines deprived of androgens, in prostate tumor xenografts in castrate mice, and in CRPC patients. Knockdown or inhibition of AKR1C3 resulted in suppression of tumor cell growth within a castrate environment and a decrease in intra-tumoral testosterone production in castrated nude mice induced by androstenedione[5-13]. Yepuru et al. have identified that AKR1C3 is also a unique AR-selective coactivator to promote CRPC growth and AKR1C3-selective competitive inhibitors inhibit this coactivator function[14]. Moreover, AKR1C3 is implicated in resistance to abiraterone and enzalutamide therapies and enzalutamide resistance *in vitro* and *in vivo* can be overcome with AKR1C3 competitive inhibitors[7, 8]. Collectively, these data suggest that AKR1C3 inhibition may have distinct advantages over the current therapeutics for the treatment of CRPC.

Considerable efforts have been invested into the discovery of compounds inhibiting AKR1C3 first for research purposes, but later also for therapeutic applications[1, 15, 16 17-23]. Penning et al. have extensively studied the inhibitory activities of nonsteroidal anti-inflammatory drugs (NSAIDs) and discovered N-phenylanthranilate and indomethacin analogs as AKR1C3 inhibitors with high selectivity versus COX-1,2[17-23]. The high-throughput screening conducted by Jamieson et al. identified 3-(3,4-dihydroisoquinolin-2(1H)-ylsulfonyl)benzoic acid as a new carboxylate inhibitor of AKR1C3 [24]. Several non-carboxylate inhibitors including isoquinolines, morpholylureas, pyrrolidine, and indole derivative have also been reported[14, 25-27]. At the same time, there have been significant efforts to explore the interaction of existing inhibitors with the enzyme by single-crystal techniques.

Studies conducted by us and other groups have reported 43 crystal structures of AKR1C3 in complex with different inhibitors[28-35]. The ligand binding pocket of AKR1C3 can be divided into oxyanion site, steroid channel, and three sub-pockets, SP1, SP2, and SP3[1]. Most of inhibitors are anchored to the oxyanion site by hydrogen bonding with Tyr55 and His117 and occupy the SP1 pocket, where usually result in conformational changes of Trp227, Phe306 and Phe311[15]. Nevertheless, no AKR1C3 inhibitors are currently in clinical use for the treatment of CRPC, and superior AKR1C3 inhibitors are still in need.

To seek novel AKR1C3 inhibitors, in the current study, we conducted a screening on an in-house compound library consisting of 298 small molecules by using enzymatic assay. Nine inhibitors were identified with new scaffolds compared to the current AKR1C3 inhibitors. Preliminary SAR studies were performed on the best compound and identified **19d** as the most potent AKR1C3 inhibitor with an IC_{50} of 0.160 μM among the synthesized 23 6-Amino-4-phenyl-1,4-dihydropyrano-[2,3-c]pyrazole-5-carbonitriles. Crystal structure, molecular docking, together with binding free-energies and per-residue contributions studies revealed a new insight into the molecular basis for selective inhibition of AKR1C3, which would be helpful in future design and optimization of new AKR1C3 inhibitors.

2. Materials and methods

2.1. Enzyme preparation and inhibition assays

Human recombinant AKR1C1 and AKR1C3 were expressed in the *E. coli* BL21 (Condon Plus) and were purified using the procedures as described before[34]. These enzymes *in vitro* reduce 9,10-phenanthrenequinone (PQ) with high catalytic efficiency in the presence of the coenzyme NADPH. Initial velocities were determined with a Flex Station® 3 Multi-Mode Microplate Reader (Molecular Devices) by measuring the decrease in NADPH emission of 460 nm with an excitation of 340 nm. The potency of the compounds was determined by their ability to inhibit the reduction reaction. The volume of the reaction mixture was 100 μL that contained 0.1 M phosphate buffer (pH = 6.0), 0.15 mM NADPH, 8.0 μM PQ, 0.33 μM AKR1C3 or 0.39 μM AKR1C1, and 1% DMSO with or without compound. Screening was carried out at 25 μM compounds and IC_{50} value were measured for a strong inhibition corresponding to more than 50% AKR1C3 inhibition. Selectivity towards AKR1C1 was further determined for the most promising compounds with IC_{50} less than 5.0 μM.

2.2. Chemistry

As shown in Scheme 1-2, we developed an efficient route to obtain the expected 6-amino-4-phenyl-1,4-dihydropyrano[2,3-c]pyrazole-5-carbonitriles **1**, **13a-k**, and **19a-l**. Our initial efforts focused on synthesis of C4-substituted and N1-substituted derivatives from 6-amino-4-phenyl-3-propyl-1,4-dihydropyrano[2,3-c]pyrazole-5-carbonitrile (Schemes 1). Ethyl 3-oxohexanoate in ethanol or glacial acetic acid was treated with the appropriate hydrazine to afford the N-substituted-3-propyl-1H-pyrazol-5(4H)-ones (**12a-g**), respectively[36, 37] Then, 6-amino-4-phenyl-3-propyl-1,4-dihydropyrano[2,3-c]pyrazole-5-carbonitriles **1** and **13a-k** were respectively synthesized by reaction of **12a-g**, aldehydes, and malononitrile in ethanol. Compounds **19a-l** were synthesized through the route outlined in Scheme 2. Meldrum's acid was reacted with acyl chloride in the presence of CH_2Cl_2 at 0 °C using pyridine as a base to afford the **16a-l**, which was then alcoholysis in ethanol to get the β-ketoester **17a-l**[38]. Finally, use the same procedure as scheme 1 to obtained the target compounds 6-amino-4-phenyl-1,4-dihydropyrano-[2,3-c]pyrazole- 5-carbonitriles **19a-l,** respectively.

Scheme 1. Synthesis of compound **1** and **13a-k**[a]

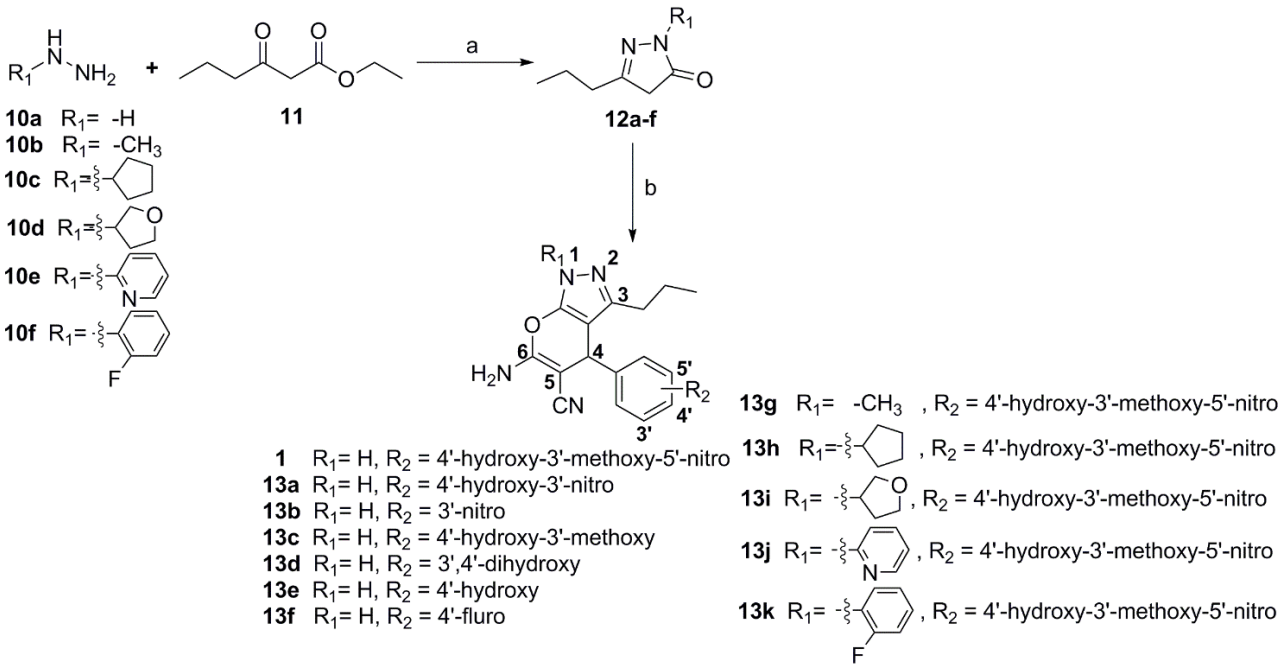

[a]Reagents and conditions: (a) hydrazine, EtOH, 70 °C, 2 h; or AcOH, AcONa, reflux 12 h; (b) aldehyde, malononitrile, piperidine, EtOH, 70 °C, 1 h.

To avoid interference of false positive compounds with our subsequent study, PAINS screening of the designed compounds was performed using an online program (i.e., "PAINSRemover", http://www.cbligand.org/PAINS/), and all the compounds passed the filter[39].

Scheme 2. Synthesis of compound **19a-l**[a]

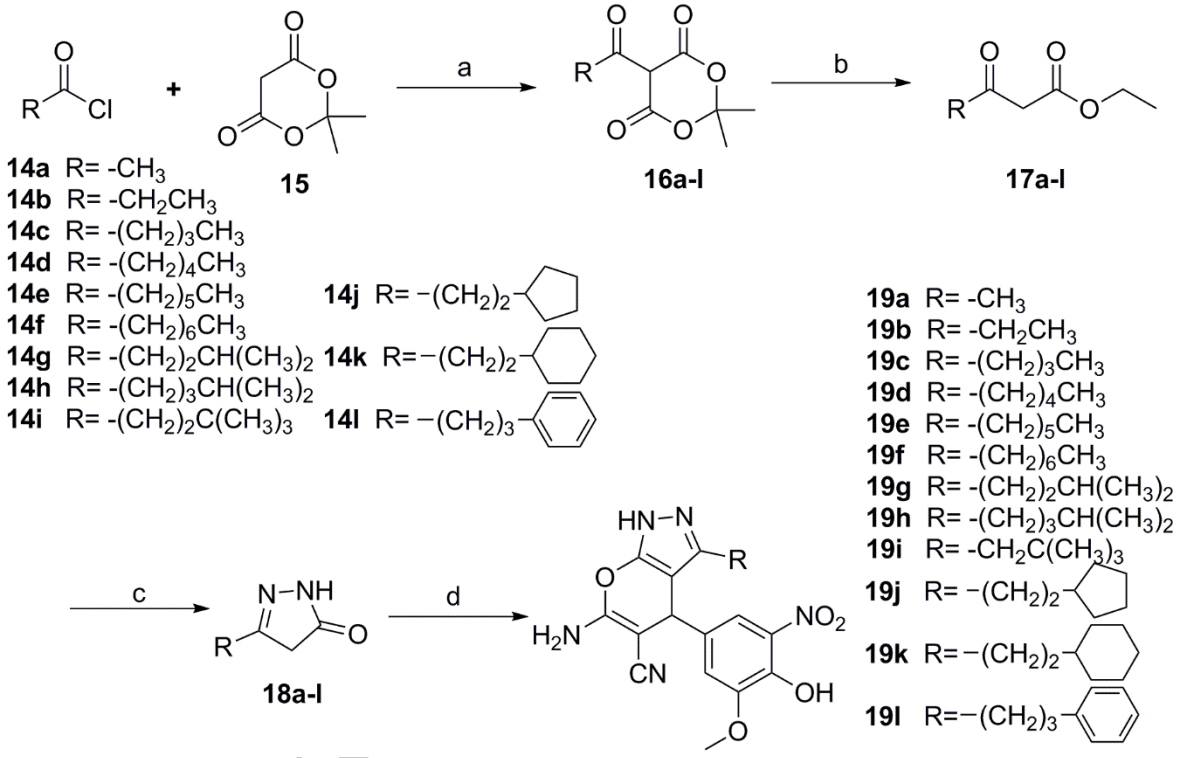

[a]Reagents and conditions: (a) pyridine, CH_2Cl_2, 0 °C, 30 min, r.t., 12 h; (b) EtOH, reflux, 4 h; (c) hydrazine, EtOH, 70 °C, 2 h; or AcOH, AcONa, reflux 12 h; (d) aldehyde, malononitrile, piperidine, EtOH, 70 °C, 1 h.

2.3. Crystallization and structure determination

Crystallization of AKR1C3/AKR1C1-$NADP^+$-inhibitor complex was achieved by soaking the AKR1C1/AKR1C3-$NADP^+$ crystals in a saturated solution of the inhibitor. AKR1C3/AKR1C1-$NADP^+$ crystals were obtained using hanging drop vapor diffusion method at 298 K. The drops were prepared by mixing 2.0 µL protein-$NADP^+$ mixture with 2.0 µL reservoir solution. AKR1C3-$NADP^+$ crystals appeared in drops containing 0.1 M MES (pH 6.0), 15-20% (w/v) PEG 8K, 0.14 M NaCl, while AKR1C1- $NADP^+$ crystals grew in drops consisting 0.1 M Hepes (pH 7.3), 23-27% PEG 4K, 10 mM $CaCl_2$, 0.4 M NaCl.

X-ray data were recorded on our in-house Oxford Diffraction Xcalibur Nova diffractometer and processed with the program *CrysAlis Pro*. The structures were built with *Phaser* by using structure of 4FAM (AKR1C3) or 3NTY (AKR1C1) as a model for molecular replacement, and refined with the program *Phenix* and *Coot*[40, 41]. *Grade Web Server* was used to generate the coordinate and restraint for the inhibitor. Data collection and refinement statistics are shown in Table S1. The coordinate data were deposited in the Protein Data Bank with accession numbers of 6A7A, 6A7B and 6IJX. Related figures were produced using *PyMOL*.

2.4. Molecular docking, molecular dynamics simulations and binding free energy calculations

Molecular docking was performed using CDOCKER module embedded in Accelrys Discovery Studio 2.5.5. The crystal structures presented in the present paper were used as the receptor. All the water molecules and ligands were removed from the target protein except cofactor $NADP^+$ and the water molecules were found to play an important role in receptor–ligand interactions (See 3.3). A spherical region with a radius of 10 Å was constructed as the binding site, based on the location of the co-crystallized ligand. The receptor and the ligands were typed with CHARMm force field and Momany-Rome partial charges. Other input parameters were set as their default options. The original ligand was re-docked into the X-ray protein to verify the dock procedure. An RMSD less than 1.0 Å between the crystal and docked conformations was considered desirable docking protocol.

The complexes obtained from X-ray or molecular docking was subject to the molecular dynamics (MD) simulation and subsequent binding free energy calculations using the sander module of Amber 14. The detailed parameters used in this study were similar to those in our previous studies[42]. The system was initially energy-minimized using steepest descent method followed by conjugated gradient method in the presence of positional restraints on both protein and ligand. After heated to 300 K with positional restraints for the protein, 8 ns production simulations were carried out after 100 ps equilibration simulations. Crystal water molecules mediating hydrogen bonds between the ligand and receptor were kept during the MD simulation. RMSD for the backbone atoms was monitored to validate the stability of the complex system. The binding free energies (ΔG_{bind}) were calculated with MM-GBSA approach using the final 1 ns of MD trajectories, which was well-equilibrated[43-47]. To obtain a detailed view of interactions between the ligand and the receptor,

the total free energy were then decomposed to each residue with the MM-GBSA method.

3. Results and discussion

3.1. In-house library screening identified 1 as AKR1C3 inhibitor with completely novel molecular scaffold

To identify AKR1C3 inhibitors with new scaffold, we screened 298 compounds at 25 μM in triplicate from our in house library. Twenty compounds showed more than 50% inhibition towards AKR1C3. Out of these compounds, 3 compounds produced high fluorescence, 5 compounds were poorly soluble in the aqueous buffer, and IC_{50} values for these compounds were unable to be assayed in our assay system. Among 12 compounds assayed, there were 3 steroids whose analogues were already identified as AKR1C3 inhibitors by others (data not shown). The active compounds having novel scaffolds for AKR1C3 inhibitors are summarized in Table 1, together with their inhibitory activity and selectivity for those with the IC_{50} values < 5.0 μM.

Nine structurally diverse compounds were identified in the present screening with the IC_{50} values covering a broad range from 0.227 μM to 24.2 μM. Among them, two compounds showed an IC_{50} values < 5.0 μM towards AKR1C3. Compound **2** with an IC_{50} value of 1.46 μM is a pyrimidine derivative. For its relatively high IC_{50} value and complicated chemical structure, we didn't pay much attention to it. The best one (compound **1**) showed a very low IC_{50} value of 0.227 μM with a slight selectivity towards AKR1C1 (0.411 μM, see the explanations in 3.2). Compared to current AKR1C3 inhibitors, 1,4-dihydropyrano[2,3-c]pyrazole derivative **1** has a completely novel scaffold, which is much more compact and rigid implying different inhibition mode may exist. Besides, 1,4-dihydropyrano[2,3-c]pyrazoles have been found to have antimicrobial, insecticidal, anti-inflammatory, molluscicidal, and Chk1 kinase inhibitory activities[36]. The chemistry on 1,4-dihydropyrano[2,3-c]pyrazoles have also received remarkable interest and some efficient synthetic routes have been reported using commercially available materials with high diversity [36, 48]. Therefore, it can be concluded that wide varieties of substituents on 1,4-dihydropyrano[2,3-c]pyrazole core could be easily achieved and therefore generating novel promising AKR1C3 inhibitors.

Table 1. Structures and inhibitory activities of AKR1C3 inhibitors with novel scaffolds

No.	Structure	Inhibitory activity (IC_{50}, μM)	
		AKR1C3	AKR1C1
1	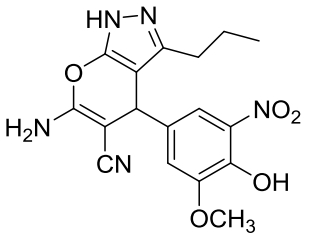	0.227±0.013	0.411±0.013
2	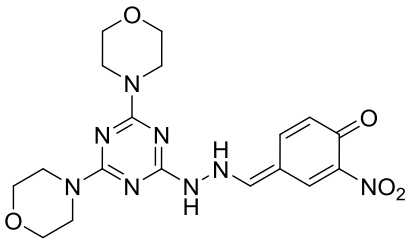	1.46±0.29	9.87±1.77
3	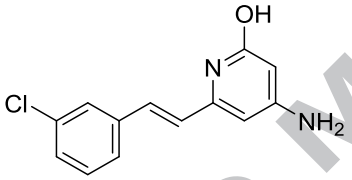	5.54±1.66	-
4	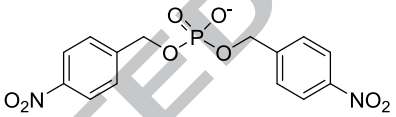	7.22±1.90	-
5	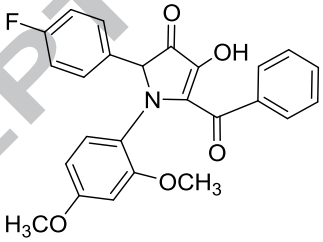	7.80±0.14	-
6	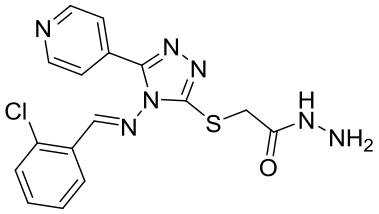	14.8±2.9	-
7	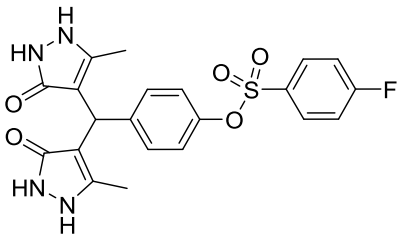	15.2±2.4	-

8	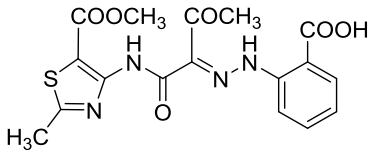	15.5±2.9	-
9	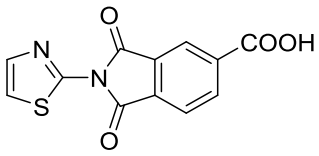	24.2±5.1	-
Meclofenamic acid[a]	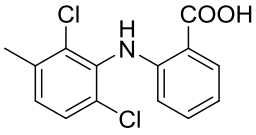	0.512±0.080(0.54[b])	0.740±0.065(3.16[b])

[a]Used as a positive control;

[b]IC_{50} values taken from reference[24].

3.2. Preliminary structure activity relationship investigations

Inspection of the reported crystal structures of AKR1C3-$NADP^+$-inhibitor showed that the carboxylate/carbonyl group on most of the known inhibitors often provides the basic anchorage of the inhibitor to the oxyanion site by hydrogen bonding with the catalytic tetrad members Tyr55 and His117. The anchorage may be not obligated but apparently beneficial for the high binding affinities of the current AKR1C3 inhibitors. Thus, we proposed a hypothesis that the nitro group (on C4-phenyl substituent) could serve as the anchor and play a role in strong inhibition of **1** towards AKR1C3. As seen from Table 2, removal of nitro group (**13c**) resulted in great decrease in the inhibitory activity. However, 3´-nitrophenyl at C4-position led to loss of inhibition of **13b**. Crystal structure of 4wdt showed an example of hydrogen bonding to the catalytic residues by a combination of nitro and hydroxyl groups, which would suggest that both of nitro and hydroxyl group may be important for retaining high binding affinity towards AKR1C3. **13a** with 3´-nitro-4´-hydroxylphenyl was thus synthesized, which as expected displayed comparable inhibitory activity to compound **1**.

Table 2. SAR of phenyl-substituted for inhibition of AKR1C3 and AKR1C1

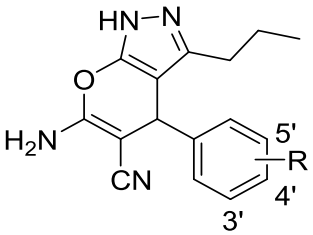

Cpd.	R	Inhibitory activity(IC_{50}, μM)	
		AKR1C3	AKR1C1
13a	4′-OH-3′-NO_2	0.278±0.054	0.661±0.125
13b	3′-NO_2	> 25	> 25
13c	4′-OH- 3′-OMe	16.5±3.8	2.49±0.02
13d	3′,4′-diOH	3.96±0.42	5.09±1.45
13e	4′-OH	6.73±0.79	3.51±1.19
13f	4′-F	> 25	> 25

Analogues sets around 1,4-dihydropyrano[2,3-c]pyrazole core were developed for the purpose of probing the interaction in the SP pockets, which usually relate with inhibitor selectivity in AKR1Cs. There are two closely related isoforms of AKR1C3 (AKR1C1 and AKR1C2), which are involved in DHT inactivation, their inhibition may increase the androgenic signal[1]. Thus, it will be necessary to inhibit AKR1C3 selectively for the treatment of CRPC. Since only a single residue is different at their respective active site, AKR1C1 inhibitors could potentially also inhibit AKR1C2. Selectivity over AKR1C1 for the compounds was evaluated. As seen in Table 3, substituents at N1-position appear to be disfavored to the inhibitory activity (**13g-13k**) towards both of AKR1C3 and AKR1C1. The least active compound of this set was **13j**, with a pyridyl substitution at N1-position, which was less potent than **1** about 22- and 6-fold for AKR1C3 and AKR1C1, respectively. By contrast, a range of substituents at C3-position seems to be very well tolerated, as many compounds exhibit comparable or superior inhibitory activities to the parent **1** (Table 4). However, both the short and long chain substituents would decrease the potency. Overall, the most potent compound **19d,** with pentyl substitution at the C3-position, had an IC_{50} of 0.160 μM. **19d** is also the most selective compound among all the molecules, which illustrated about 3.3-fold selectivity between AKR1C3 and AKR1C1.

Table 3. SAR of N1-substitutions for inhibition of AKR1C3 and AKR1C1

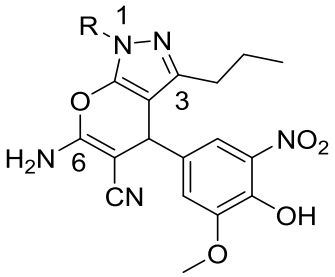

Cpd.	R	Inhibitory activity (IC_{50}, μM)	
		AKR1C3	AKR1C1
13g	-CH_3	0.510±0.091	0.462±0.082
13h	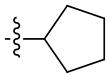	1.83±0.37	1.05±0.18
13i	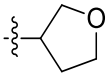	0.778±0.044	1.09±0.07
13j	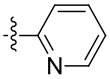	5.05±0.56	2.52±0.45
13k	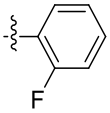	0.683±0.157	1.27±0.16

Table 4. SAR of C3-substitutions for inhibition of AKR1C3 and AKR1C1

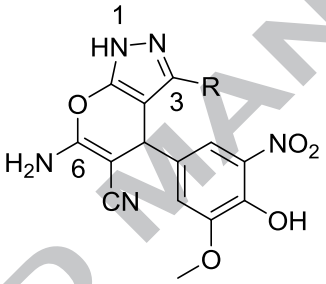

Cpd.	R	Inhibitory activity (IC_{50}, μM)	
		AKR1C3	AKR1C1
19a	-CH_3	0.533±0.095	0.487±0.087
19b	-CH_2CH_3	0.255±0.025	0.790±0.005
19c	-$(CH_2)_3CH_3$	0.213±0.020	0.810±0.046
19d	-$(CH_2)_4CH_3$	0.160±0.028	0.531±0.095
19e	-$(CH_2)_5CH_3$	0.168±0.011	0.534±0.060
19f	-$(CH_2)_6CH_3$	0.684±0.014	1.20±0.03
19g	-$(CH_2)_2CH(CH_3)_2$	0.676±0.158	0.870±0.042
19h	-$(CH_2)_3CH(CH_3)_2$	0.730±0.067	1.21±0.10
19i	-$CH_2C(CH_3)_3$	0.480±0.047	0.844±0.126
19j	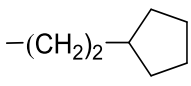	0.237±0.042	0.433±0.077
19k	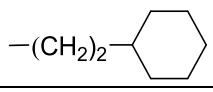	0.287±0.033	0.443±0.077

19l	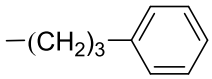	0.469±0.084	0.801±0.144

3.3. The unique mode of binding between 1 and AKR1C3

To understand how the potency is achieved, we determined the structure of compound **1** bound to AKR1C3 by soaking it into the AKR1C3-$NADP^+$ crystals. Electron density for compound **1** was clearly observed in the active site region. As shown in figure 1A, compound **1** binds to the oxyanion site, SP2 and SP3 pocket, and the hydroxyl group forms hydrogen bonds to Tyr55 (2.6 Å) and His117 (2.7 Å). The methoxy and nitro group also form hydrogen bond to Tyr55 or His117. It is firstly observed that hydroxyl, methoxy and nitro groups together anchor the inhibitor to the oxyanion site. However, as seen from the SAR results, compared to methoxy group, it appears that nitro group plays a more important role in the binding. A comparison of their chemical properties identified an important difference between them, i.e. only nitro group being one of the strongest electron-withdrawing groups. Because of this property, O−H is expected to be more acidic and be a better H-bond acceptor, thus mimicking the carboxylate group. The 1,4-dihydropyrano[2,3-c]pyrazole core enters into the SP2 and SP3 pocket, which is defined by Trp86, Leu122, Ser129, and Phe311, and by $NADP^+$, Tyr24, Glu192, Ser221 and Tyr305, respectively, and in which lots of hydrogen bond interactions were formed via water molecules. All the atoms on the core that are capable of forming hydrogen interactions are involved in this hydrogen bond net with $NADP^+$, Tyr24, Gln192, Tyr216, Ser217, Gln222, Asp224, and Tyr319. It is likely that hydrogen bond interactions contribute largely to the inhibitory potency of **1**.

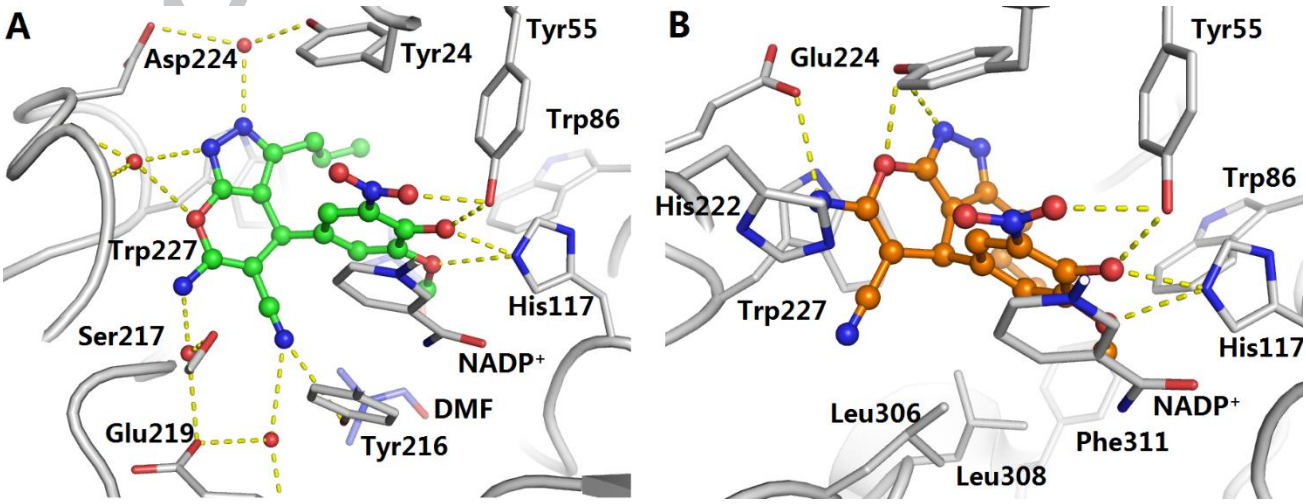

Figure 1. Crystal structures of **1** bound to AKR1C3 (A) and AKR1C1 (B). Carbon atoms for the

protein and $NADP^+$, DMF, and **1** are colored gray, slate, and green (in AKR1C3)/orange (in AKR1C1), respectively. Key hydrogen bonds are represented as dotted lines.

The overall structure of AKR1C3-$NADP^+$-**1** is similar to the crystal structure of AKR1C3-$NADP^+$-indomethacin (PDB entry 1S2A) as assessed by inhibitor binding position and the side chain conformations of mobile residues Phe306, and Phe311[30]. Both of them induce a rotation of Phe306, in concert with Phe311, thereby exposing SP3 pocket. However, a more significant rotation is seen in the mobile residue Trp227 in structure of AKR1C3-$NADP^+$-**1**. Trp227 undergoes an approximately 200° rotation from the indomethacin or acetate (PDB entry 1S1P) containing structures. The broad flips of Phe306, Trp227 and Phe311 dramatically enlarged the binding pocket and made the active site more accessible. To our knowledge, only bimatoprost (PDB entry 2F38) and PGD_2 (PDB entry 1RY0) with much long side chains induced similar flips in these mobile residues[28, 35]. Compared to bimatoprost and PGD_2, compound **1** is more compact and "closed". Thus, while bimatoprost and PGD_2 enter deeply into SP1 and SP2 pocket, compound **1** binds mainly in the SP3 pocket, and allowed SP1 and SP2 pockets to be occupied by solvent DMF. According to the above analysis, we can conclude that the binding pattern of **1** is fairly distinct from those of previously reported inhibitors and there is enough room for compound **1** to improve the binding affinity by fully occupying the SP pockets.

3.4 Induced-fit conformational changes of 1 upon binding to AKR1C1

As proposed by Byrns et al., selectivity in AKR1Cs can be gained by taking advantage of the structural differences in Phe306 [15]. Because the corresponding residue in AKR1C1 and AKR1C2 (Leu306) has a more rigid side chain that would clash with inhibitors entering the SP3 pocket, such as selective AKR1C3 inhibitor indomethacin. However, as a SP3 pocket binding inhibitor, compound **1** displays comparable inhibition toward AKR1C1. Crystal structure of compound **1** bound to AKR1C1-$NADP^+$ was then determined to uncover the potential mechanism. As seen from figure 1B, compound **1** binds to AKR1C1 in a similar manner to AKR1C3 by interring with residues from oxyanion site, SP2 and SP3 pocket. However, to avoid the clash with Leu306, compound **1** moves significantly closer to SP2 pocket. The closest contacts between the attached propyl group and Phe311 from SP2 pocket were 3.8 Å and 8.0 Å for AKR1C1 and AKR1C3, respectively (Figure 2A), and, hydrogen bond net in the SP3 pocket is formed directly to the residues of AKR1C1 but via the

water molecules in AKR1C3. In addition, compound **1** was found to undergo a slight rotation. The bicyclic core displays about 11° torsion difference from the benzene ring plane in the two structures (Figure 2B).

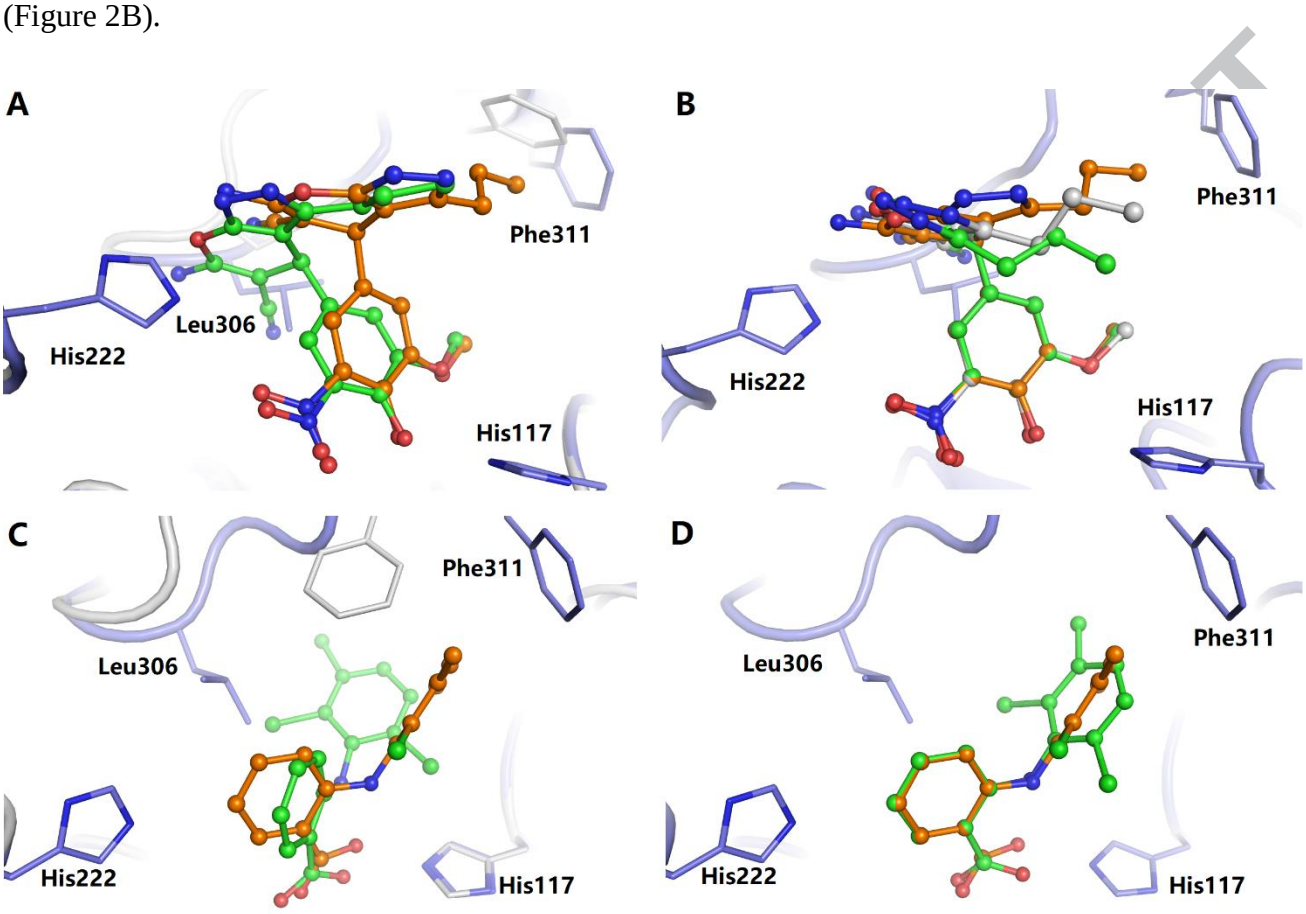

Figure 2. Superimposition of AKR1C3 and AKR1C1 by residues (A, C) and inhibitors (B, D) showed that both compound **1 (A, B)** and meclofenamic acid (C, D) undergo conformation changes to suite binding interface. Surrounding residues are represented by gray and slate sticks for AKR1C3 and AKR1C1, respectively. Binding poses are colored in green (in AKR1C3) or orange (in AKR1C1), while the preferred conformation of compound **1** is rendered as gray ball and stick model.

It is noted that pH-dependent binding modes were observed in indomethacin-AKR1C3 crystals[21, 32]. As the presented crystal structures were obtained from different pH. The observed different binding poses of compound **1** are also pH dependent? The pH-dependent enzymatic inhibition study indicated that compound **1** is more potent at pH 7.5 (IC_{50} = 0.0869 ± 0.0274), which may result from the decreased enzymatic activity. However, indomethacin showed lower inhibitory activity at pH 7.5 (IC_{50} = 4.30 ± 1.07) than at pH 6.0 (IC_{50} = 2.12 ± 0.79). It suggested pH likely would have a great impact on indomethacin binding, but it does not affect compound **1** binding that

much. In addition, molecular modeling predicted a preferred conformation of compound **1** that differs from the conformations in the two structures. Thus, it is reasonable to assume that compound **1** reshapes itself to suit different binding interfaces. As shown in Figure 2C and 2D, the crystal structures obtained from similar pH showed that, to avoid the clash with Leu306, meclofenamic acid (MCF) also adopts a different binding poses when binds to AKR1C1 and AKR1C3 (PDB entry 3R6I), which clearly explains the lack of isoform specificity reported for this ligand. These findings suggested that it might also be necessary to consider the conformational changes of the inhibitor in the rational design of selective AKR1C3 inhibitors, which would make AKR1C3 inhibitors discovery more difficult. It may be useful in estimating the specificity of the lead and the designs, if the two binding interfaces were both taken into account. For example, as shown in figure 3, N-Phenylanthranilic acid based AKR1C3 inhibitors flufenamic acid (FLF) and BT9 showed high similarities in their chemical structure, AKR1C3 inhibitory activity and binding pattern, which is not sufficient to explain their big difference in specificity (selectivity ratio of 6 and 378, respectively)[24, 29]. However, when these two compounds docked into AKR1C1, many different features were observed. FLF binds to AKR1C1 in a similar manner to MCF, whereas BT9 moves to an outer area of the protein where little strong interactions can be formed. Thus, FLF gave much better docking scores than BT9, which explains their big difference in AKR1C1 binding affinity.

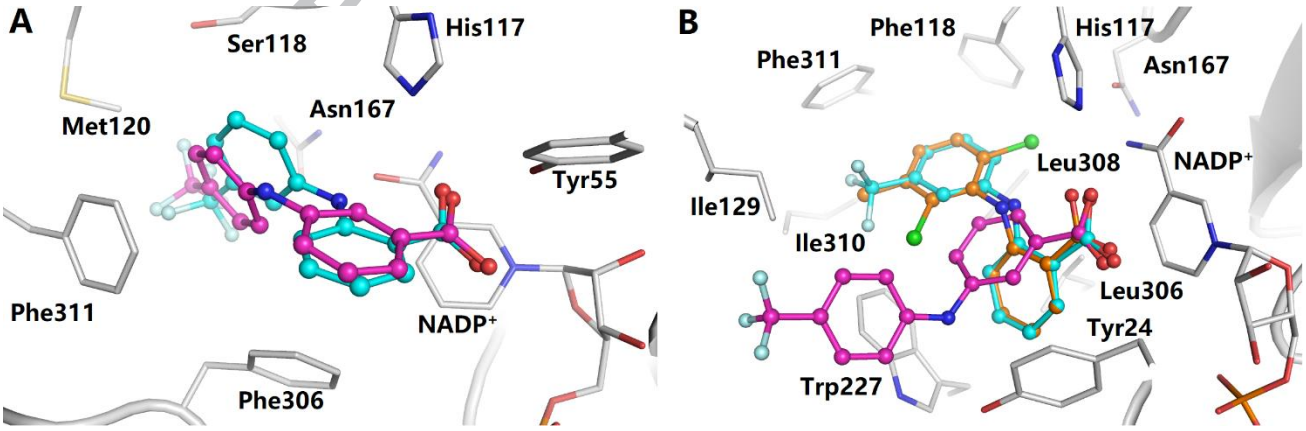

Figure 3. Structures of flufenamic acid (FLF) and BT9 bound to AKR1C3 (A) and AKR1C1 (B) help to explain their big difference in specificity. Carbon atoms for the protein, FLF, BT9 and meclofenamic acid are represented by gray, cyan, magenta and orange, respectively.

3.5. Energy analysis for the binding features of 1

To comprehensively understand the binding features of **1**, the MM-GBSA method was applied to estimate the binding free energy (ΔG_{bind}) and the contribution of key residues in the binding of **1** with AKR1C3 and AKR1C1. Crystal water molecules discussed above were kept to understand the role of water molecules in the binding. As shown in Table 5, the ΔG_{bind} values for **1** in the binding of AKR1C3 and AKR1C1 are -37.02 and -37.08 kcal/mol, respectively. For both AKR1C3-$NADP^+$-**1** and AKR1C1-$NADP^+$-**1** complexes, electrostatic and van der Waals interactions are the major favorable contributors for the binding, whereas the polar solvation energies have positive values and led to an overall positive value of the solvation free energy, indicating it opposes binding. Furthermore, the electrostatic interactions value is slightly larger than that of the van der Waals interactions.

Table 5. The binding free energies for AKR1C3 and AKR1C1 complex systems by MM-GBSA method

Energies (kcal/mol)	ΔE_{ele}	ΔE_{vdW}	ΔG_{polar}	ΔG_{nonpl}	ΔG_{gas}	ΔG_{sol}	ΔG_{bind}	IC_{50} (μM)
AKR1C3								
1	-45.78±2.75	-38.60±3.90	51.38±2.14	-4.01±0.09	-84.38±4.24	47.36±2.15	-37.02±3.34	0.227±0.013
19d	-47.90±5.02	-44.97±2.69	57.18±3.48	-3.98±0.08	-92.87±5.11	53.19±3.49	-39.68±2.90	0.160±0.028
19l	-45.50±4.72	-47.00±3.03	64.57±2.66	-4.39±0.07	-92.50±4.65	60.17±2.66	-32.33±3.84	0.469±0.084
13i	-16.39±4.48	-51.51±2.67	41.92±3.09	-4.63±0.07	-67.90±5.02	37.29±3.08	-30.61±3.47	0.778±0.044
AKR1C1								
1	-45.20±4.61	-44.26±3.07	57.17±3.39	-4.05±0.09	-89.47±4.23	52.39±3.02	-37.08±3.88	0.411±0.013
19d	-49.202±4.40	-44.85±2.59	61.22±3.38	-4.12±0.07	-93.88±4.88	56.51±3.01	-36.71±3.04	0.531±0.095
19l	-38.53±3.94	-55.08±3.16	62.10±3.26	-4.60±0.12	-93.61±5.03	57.49±3.23	-36.12±3.16	0.801±0.144
13i	-42.59±6.61	-47.89±3.28	59.99±5.52	-4.46±0.17	-90.47±7.07	55.53±5.52	-34.94±3.40	1.09±0.07

ΔE_{ele}/ΔE_{vdW}: Electrostatic/van der Waals contributions;
ΔG_{polar}/ΔG_{nonpl}: Polar/nonpolar contributions to solvation;
$\Delta G_{gas} = \Delta E_{ele}, + \Delta E_{vdW}$;
$\Delta G_{sol} = \Delta G_{polar} + \Delta G_{nonpolar}$;
$\Delta G_{bind} = \Delta G_{gas} + \Delta G_{sol}$, the binding free energies without entropic contribution.

As shown in Figure 4, the residues with the most favorable contributions (lower than −1.0

kcal/mol) are located at the active site. These residues were considered as key residues which included Tyr24, Tyr55, Gln/His222, Asp/Glu224, Trp227, Phe/Leu306 and $NADP^+$. As expected, $NADP^+$ in both AKR1C3 and AKR1C1 are suggested to have high affinity with **1** by forming strong electrostatic interactions. Other residues are mostly those involved in the hydrogen bond interactions with **1**, which imply the importance of the hydrogen bond interactions that facilitate the electrostatic energy contributions. Notably, the contributions of Trp227 are also relatively higher than for other residues. The further investigation of the binding patterns shows that Trp227 is involved in π-π stacking interactions with **1** in both AKR1C3 and AKR1C1. The key residues comparison between AKR1C3 and AKR1C1 identified some different interacting points. Leu308 is a key residue for the binding to AKR1C1, whereas water molecules are important for AKR1C3 binding, which agrees with the results from the crystal structures.

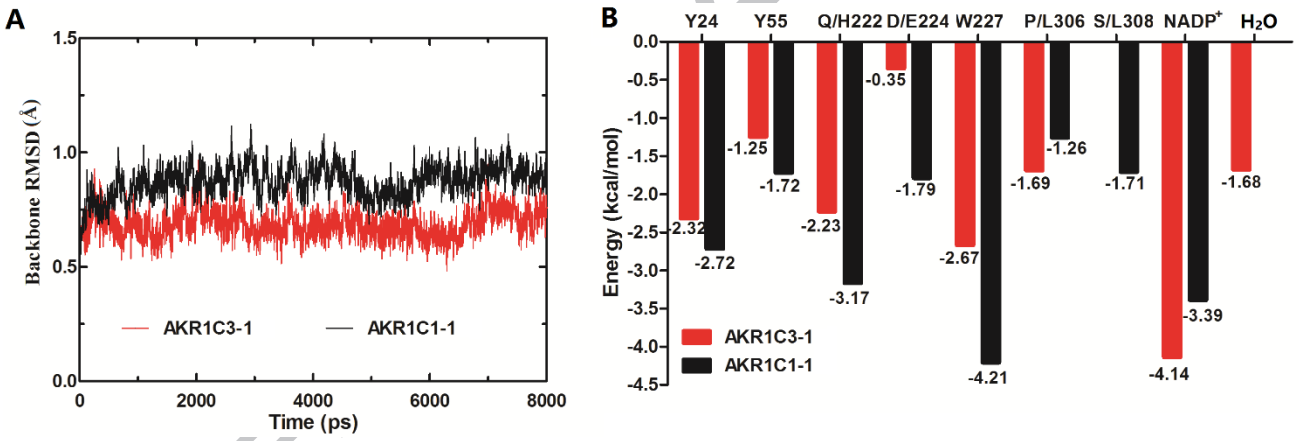

Figure 4. Molecular dynamics simulations results of **1**. (A) Cα RMSD plots of AKR1C3-**1** (red) and AKR1C1-**1** systems (black). (B) The inhibitor–residue interaction spectrum between **1** and the important residues for AKR1C3 (red) and AKR1C1 (black).

3.6. Binding features of the reprehensive derivatives 13i, 19d and 19l

To better understand the structural basis for the potency and selectivity of pyranopyrazoles, the binding modes of three chosen representative derivatives **13i**, **19d** and **19l** were investigated using molecular docking and molecular dynamics simulations. Coordinates of the target protein were obtained from the co-crystal structure of AKR1C3/C1-$NADP^+$-**1**. We firstly re-docked the original ligand to the crystal structure that generated an RMSD between the docked and crystal poses of 0.2224 and 0.1108 for AKR1C3 and AKR1C1, respectively, which validates the reliability of the

docking procedures.

As shown in Figure 5A, **19d** would mimic the binding pattern of compound **1** at the greatest extent. It thus observed that **19d** makes similar interactions with the key residues defined in 3.5 including Tyr24, Tyr55, Gln222, Asp224, Trp227, Phe306 and $NADP^+$. Moreover, interactions between the pentyl and residues Trp227 and Trp86 could be stronger because of their closer contact, which would contribute to the higher IC_{50} value of **19d** than that of compound **1**. However, **13i** and **19l** moves away from the crystal position of compound **1** to some extent as shown in Figure S1A, which would lead to the loss of interactions from some key residues that result in their weaker potencies. MM-GBSA estimated the ΔG_{bind} values of -30.61, -39.68 and -32.33 kcal/mol for **13i**, **19d**, and **19l**, respectively, which were consistent with the results from the molecular docking.

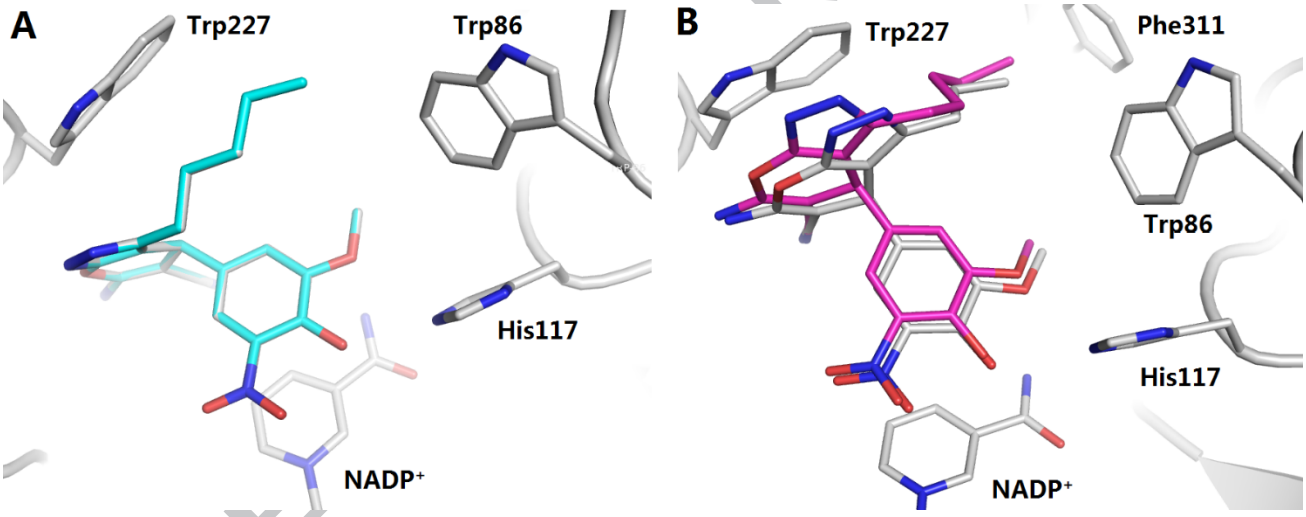

Figure 5. Comparisons on the binding patterns of **1** and **19d** to AKR1C3 (A) and AKR1C1 (B). Carbon atoms for the protein, $NADP^+$ and **1** are displayed as gray, while 19d is represented by cyan (in AKR1C3) or magenta (in AKR1C1) carbon atoms.

19d binding to AKR1C1 were shown in Figure 5B, which illustrated **19d** would move slightly away from the crystal position of compound **1** to avoid the clash with Phe311 from SP2 pocket. This result is consistent with the slightly decreased potency of **19d** towards AKR1C1. It was thus observed that **19d** exhibited higher selectivity than compound **1**. Docking results of **13i** and **19l** towards AKR1C1 were shown in figure S1B, which showed the binding patterns having fewer interactions that agree with their weaker potency. Also, the estimated ΔG_{bind} values were also found to be in agreement with their potencies.

3.7. Molecular basis for the inhibitory potency and selectivity of pyranopyrazoles

Nitro and hydroxyl group on the C4-phenyl ring are required to boost the potency of the compounds by anchoring the inhibitor to the oxyanion site, whereas substituents at N1- and C3-position of the core would affect the potency and selectivity. Increasing the length of the alkyl substituents on C3-position would favor the enhancement of the potency and selectivity by better occupying the relatively larger SP2 pocket of AKR1C3 but being pushed by Phe311 of AKR1C1. However, too long or too bulky C3-substituents couldn't even be accommodated by the SP2 pocket of the AKR1C3. Thus, **19d** and **19e** having pentyl or hexyl group at this position displayed both highest inhibitory activity and selectivity of the set. Furthermore, our results suggested that SP2 pocket could be utilized to just slightly elevate the potency and selectivity of **1**. By contrast, substituents on N1-postion would extend to the entrance of the binding pocket of AKR1C3 and AKR1C1 that resulted in loss of some interactions. It explains why no apparent improved potency and selectivity for AKR1C3 was observed for compounds **13j-13k**. Crystal and MD studies suggested that the hydrogen-bond network formed in the SP3 pocket contribute greatly to the potent inhibitory activity of compound **1**, and thus modifications on the related positions would be unfavorable. Taken together, SP1 pocket would be suggested to be utilized to further improve the binding affinity and selectivity of the current AKR1C3 inhibitor. This hypothesis supported by the orientation of the methoxy group of compound **1** to the SP1 pocket, which could thus be replaced to fully occupy the SP1 pocket. AKR1C3 and AKR1C1 docking studies have already confirmed our proposal and selective pyranopyrazole AKR1C3 inhibitors are currently being developed by our group.

4. Conclusions

AKR1C3 plays a critical role in androgen biosynthesis and in the development of CRPC, making it a promising drug target. Using an AKR1C3 enzymatic assay to evaluate our in-house chemical library, we identified 6-amino-4-phenyl-1,4-dihydropyrano[2,3-c]- pyrazole-5-carbonitrile derivative **1** as a potential AKR1C3 inhibitor, which exhibited both high potency and novel chemical structure from known AKR1C3 inhibitors. Consequently, twenty-three analogues of **1** were synthesized to explore the structure activity relationships that discovered sixteen compounds with an $IC_{50} < 1.0$ μM, five compounds with an $IC_{50} < 0.25$ μM. One of the most promising compound **19d**

strongly inhibits the AKR1C3 with an IC_{50} of 0.160 μM. Crystal structure studies revealed a new binding mode of compound **1**, in which hydroxyl, methoxy and nitro group at the C4-phenyl substituent together anchor the inhibitor to the oxyanion site, and the core scaffold enlarges but partially occupies the SP pockets with abundant hydrogen bond interactions. Binding free-energy and per-residue contribution studies indicate that hydrogen bonds formed in the oxyanion site and SP pocket can contribute to the high potency of pyranopyrazole analogues towards AKR1C3. In addition, to bind to the homologous protein AKR1C1, compound **1** was found to reshape itself to fit different receptors, which elucidate the molecular basis of the selectivity of pyranopyrazole derivatives and indicates that conformational changes of the inhibitor may also need to be considered in development of AKR1C3 inhibitors. These observations suggest that **19d** is a promising lead against AKR1C3 and provides a new insight into the molecular basis for future design and optimization of new AKR1C3 inhibitors.

Acknowledgements

This work was supported by the Natural Science Foundation of China (81602968, and 81602955), the Natural Science Foundation of Guangdong Province (2016A030313589, and 2016A030310144), the Medical Scientific Research Foundation of Guangdong Province (A2016201, and A2016104), Science and Technology Program of Guangzhou, China (201707010049), and Guangdong Provincial Key Laboratory of Construction Foundation (2017B030314030).

The in-house compound library was provided by Prof. Jun Xu from Research Center for Drug Discovery at Sun Yat-sen University. Also, Prof. Jun Xu has co-designed experiments, interpreted the results, reviewed and edited the manuscript, and approved the final manuscript.

References

1. Adeniji, A. O.; Chen, M.; Penning, T. M. *J Steroid Biochem Mol Biol* **2013,** *137*, 136.
2. Omlin, A.; Pezaro, C.; Gillessen, S. S. *Ther Adv Urol* **2014,** *6*, 3.
3. Chuu, C. P.; Kokontis, J. M.; Hiipakka, R. A.; Fukuchi, J.; Lin, H. P.; Lin, C. Y.; Huo, C.; Su, L. C. *J Biomed Sci* **2011,** *18*, 63.
4. Scher, H. I.; Sawyers, C. L. *J Clin Oncol* **2005,** *23*, 8253.
5. Pelletier, G. *Best Pract Res Clin Endocrinol Metab* **2008,** *22*, 223.
6. Hofland, J.; van Weerden, W. M.; Dits, N. F.; Steenbergen, J.; van Leenders, G. J.; Jenster, G.;

Schroder, F. H.; de Jong, F. H. *Cancer Res* **2010,** *70*, 1256.

7. Liu, C.; Armstrong, C. M.; Lou, W.; Lombard, A.; Evans, C. P.; Gao, A. C. *Mol Cancer Ther* **2017,** *16*, 35.
8. Liu, C.; Lou, W.; Zhu, Y.; Yang, J. C.; Nadiminty, N.; Gaikwad, N. W.; Evans, C. P.; Gao, A. C. *Cancer Res* **2015,** *75*, 1413.
9. Mitsiades, N.; Sung, C. C.; Schultz, N.; Danila, D. C.; He, B.; Eedunuri, V. K.; Fleisher, M.; Sander, C.; Sawyers, C. L.; Scher, H. I. *Cancer Res* **2012,** *72*, 6142.
10. Stanbrough, M.; Bubley, G. J.; Ross, K.; Golub, T. R.; Rubin, M. A.; Penning, T. M.; Febbo, P. G.; Balk, S. P. *Cancer Res* **2006,** *66*, 2815.
11. Hamid, A. R.; Pfeiffer, M. J.; Verhaegh, G. W.; Schaafsma, E.; Brandt, A.; Sweep, F. C.; Sedelaar, J. P.; Schalken, J. A. *Mol Med* **2013,** *18*, 1449.
12. Pfeiffer, M. J.; Smit, F. P.; Sedelaar, J. P.; Schalken, J. A. *Mol Med* **2011,** *17*, 657.
13. Downs, T. M.; Burton, D. W.; Araiza, F. L.; Hastings, R. H.; Deftos, L. J. *Cancer Lett* **2011,** *306*, 52.
14. Yepuru, M.; Wu, Z.; Kulkarni, A.; Yin, F.; Barrett, C. M.; Kim, J.; Steiner, M. S.; Miller, D. D.; Dalton, J. T.; Narayanan, R. *Clin Cancer Res* **2013,** *19*, 5613.
15. Byrns, M. C.; Jin, Y.; Penning, T. M. *J Steroid Biochem Mol Biol* **2011,** *125*, 95.
16. Penning, T. M. *Expert Opin Ther Pat* **2017,** *27*, 1329.
17. Gobec, S.; Brozic, P.; Rizner, T. L. *Bioorg Med Chem Lett* **2005,** *15*, 5170.
18. Adeniji, A. O.; Twenter, B. M.; Byrns, M. C.; Jin, Y.; Winkler, J. D.; Penning, T. M. *Bioorg Med Chem Lett* **2011,** *21*, 1464.
19. Adeniji, A. O.; Twenter, B. M.; Byrns, M. C.; Jin, Y.; Chen, M.; Winkler, J. D.; Penning, T. M. *J Med Chem* **2012,** *55*, 2311.
20. Adeniji, A.; Uddin, M. J.; Zang, T.; Tamae, D.; Wangtrakuldee, P.; Marnett, L. J.; Penning, T. M. *J Med Chem* **2016,** *59*, 7431.
21. Liedtke, A. J.; Adeniji, A. O.; Chen, M.; Byrns, M. C.; Jin, Y.; Christianson, D. W.; Marnett, L. J.; Penning, T. M. *J Med Chem* **2013,** *56*, 2429.
22. Bauman, D. R.; Rudnick, S. I.; Szewczuk, L. M.; Jin, Y.; Gopishetty, S.; Penning, T. M. *Mol Pharmacol* **2005,** *67*, 60.
23. Byrns, M. C.; Steckelbroeck, S.; Penning, T. M. *Biochem Pharmacol* **2008,** *75*, 484.

24. Jamieson, S. M.; Brooke, D. G.; Heinrich, D.; Atwell, G. J.; Silva, S.; Hamilton, E. J.; Turnbull, A. P.; Rigoreau, L. J.; Trivier, E.; Soudy, C.; Samlal, S. S.; Owen, P. J.; Schroeder, E.; Raynham, T.; Flanagan, J. U.; Denny, W. A. *J Med Chem* **2012,** *55*, 7746.
25. Heinrich, D. M.; Flanagan, J. U.; Jamieson, S. M.; Silva, S.; Rigoreau, L. J.; Trivier, E.; Raynham, T.; Turnbull, A. P.; Denny, W. A. *Eur J Med Chem* **2013,** *62*, 738.
26. Flanagan, J. U.; Atwell, G. J.; Heinrich, D. M.; Brooke, D. G.; Silva, S.; Rigoreau, L. J.; Trivier, E.; Turnbull, A. P.; Raynham, T.; Jamieson, S. M.; Denny, W. A. *Bioorg Med Chem* **2014,** *22*, 967.
27. Watanabe, K.; Kakefuda, A.; Yasuda, M.; Enjo, K.; Kikuchi, A.; Furutani, T.; Naritomi, Y.; Otsuka, Y.; Okada, M.; Ohta, M. *Bioorg Med Chem* **2013,** *21*, 5261.
28. Komoto, J.; Yamada, T.; Watanabe, K.; Takusagawa, F. *Biochemistry-US* **2004,** *43*, 2188.
29. Chen, M.; Adeniji, A. O.; Twenter, B. M.; Winkler, J. D.; Christianson, D. W.; Penning, T. M. *Bioorg Med Chem Lett* **2012,** *22*, 3492.
30. Lovering, A. L.; Ride, J. P.; Bunce, C. M.; Desmond, J. C.; Cummings, S. M.; White, S. A. *Cancer Res* **2004,** *64*, 1802.
31. Qiu, W.; Zhou, M.; Labrie, F.; Lin, S. X. *Mol Endocrinol* **2004,** *18*, 1798.
32. Flanagan, J. U.; Yosaatmadja, Y.; Teague, R. M.; Chai, M. Z.; Turnbull, A. P.; Squire, C. J. *Plos One* **2012,** *7*, e43965.
33. Amano, Y.; Yamaguchi, T.; Niimi, T.; Sakashita, H. *Acta Crystallogr D Biol Crystallogr* **2015,** *71*, 918.
34. Zhao, Y.; Zheng, X.; Zhang, H.; Zhai, J.; Zhang, L.; Li, C.; Zeng, K.; Chen, Y.; Li, Q.; Hu, X. *Chem Biol Interact* **2015,** *240*, 310.
35. Komoto, J.; Yamada, T.; Watanabe, K.; Woodward, D. F.; Takusagawa, F. *Biochemistry-US* **2006,** *45*, 1987.
36. Lehmann, F.; Holm, M.; Laufer, S. *J Comb Chem* **2008,** *10*, 364.
37. Sheng, X.; Hua, K.; Yang, C.; Wang, X.; Ji, H.; Xu, J.; Huang, Z.; Zhang, Y. *Bioorg Med Chem Lett* **2015,** *25*, 3535.
38. Davis, J. M.; Truong, A.; Hamilton, A. D. *Org Lett* **2005,** *7*, 5405.
39. Baell, J. B.; Holloway, G. A. *J Med Chem* **2010,** *53*, 2719.
40. Adams, P. D.; Afonine, P. V.; Bunkoczi, G.; Chen, V. B.; Davis, I. W.; Echols, N.; Headd, J. J.;

Hung, L. W.; Kapral, G. J.; Grosse-Kunstleve, R. W.; McCoy, A. J.; Moriarty, N. W.; Oeffner, R.; Read, R. J.; Richardson, D. C.; Richardson, J. S.; Terwilliger, T. C.; Zwart, P. H. *Acta Crystallogr D Biol Crystallogr* **2010,** *66*, 213.

41. Emsley, P.; Cowtan, K. *Acta Crystallogr D Biol Crystallogr* **2004,** *60*, 2126.
42. Huang, Y.; Liu, X.; Wu, D.; Tang, G.; Lai, Z.; Zheng, X.; Yin, S.; Luo, H. B. *Biochemistry Pharmacol* **2017,** *130*, 51.
43. Chen, F.; Liu, H.; Sun, H.; Pan, P.; Li, Y.; Li, D.; Hou, T. *Phys Chem Chem Phys* **2016**, 18, 22129.
44. Sun, H.; Li, Y.; Shen, M.; Tian, S.; Xu, L.; Pan, P.; Guan, Y.; Hou, T. *Phys Chem Chem Phys* **2014**, 16, 22035.
45. Sun, H.; Li, Y.; Tian, S.; Xu, L.; Hou, T. *Phys Chem Chem Phys* **2014**, 16, 16719.
46. Xu, L.; Sun, H.; Li, Y.; Wang, J.; Hou, T. *J Phys Chem B* **2013**, 117, 8408.
47. Hou, T.; Wang, J.; Li, Y.; Wang, W. *J Chem Inf Model* **2011**, 51, 69.
48. Li, X.; Guo, H. *Chin. J. Org. Chem.* **2012,** 32, 127.

- Substituted pyranopyrazoles as novel AKR1C3 inhibitors.
- Crystal structure revealed a unique binding pattern.
- Pyranopyrazoles change conformations to suit AKR1C3 and AKR1C1.
- Meclofenamic acid reshapes itself to fit AKR1C3 and AKR1C1.
- Conformational changes of ligand should be considered in design of AKR1C3 inhibitor.